Defining the Pathway of Worm-like Amyloid Fibril Formation by the Mouse Prion Protein by Delineation of the Productive and Unproductive Oligomerization Reactions[†]

Shweta Jain and Jayant B. Udgaonkar*

National Centre for Biological Sciences, Tata Institute of Fundamental Research, Bangalore 560065, India

ABSTRACT: Aggregation reactions of proteins leading to amyloid fibril formation are often characterized by early transient accumulation of a heterogeneous population of soluble oligomers differing in size and structure. Delineating the kinetic roles of the different oligomeric forms in fibril formation has been a major challenge. The aggregation of the mouse prion protein to form worm-like amyloid fibrils at low pH is known to proceed via a β-rich oligomer ensemble, which is shown here to be comprised of two subpopulations of oligomers that differ in size and internal structure. The relative populations of the two oligomers can be tuned by varying the concentration of NaCl present. By demonstrating that the apparent rate constant for the formation of fibrils is dependent linearly on the concentration of the larger oligomer and is independent of the concentration of the smaller oligomer, we show that the larger oligomer is a productive intermediate that accumulates on the direct pathway of aggregation from monomer to worm-like fibrils. The smaller oligomer is shown to be populated off the pathway of the larger oligomer and, hence, is not directly productive for fibril formation. The relative populations of the two oligomers can also be tuned by single-amino acid residue changes in the sequence of the protein. The different protein variants yield worm-like fibrils of different lengths, and the apparent rate of formation of the fibrils by the mutant variants is also shown to be dependent on the concentration of the larger but not of the smaller oligomer formed.

The prion protein (PrP) is a highly conserved glycoprotein, which is expressed ubiquitously in the mammalian brain specifically in neurons. The normal cellular form of the prion protein (PrP^c) is α-rich, monomeric, and soluble (*1, 2*). Its biological function is not known, although several functions have been suggested (*3, 4*). An alternative conformation of the prion protein, PrP^{Sc}, which is infectious, seems to cause a group of fatal neurodegenerative disorders, such as Creutzfeldt-Jackob disease in humans, as well as bovine spongiform encephalopathy and scrapie in animals (*1, 2, 5*). The structure and size of PrP^{Sc} are not clearly defined because of its low solubility. Nevertheless, it has been shown to be β-rich, multimeric, and resistant to protease digestion (*1, 2, 5−7*). Structural studies using electron crystallography and electron microscopy have suggested that PrP^{Sc} adopts a parallel left-handed β-helical fold (*8, 9*). PrP^{Sc} can autocatalytically convert PrP^c to its pathogenic PrP^{Sc} self (*1, 2, 5−7*). It has now become clear that prion disease can occur by amyloidogenic aggregation of the prion protein (*10*). In vitro studies have shown that the prion protein can adopt an α-rich monomeric form as well as an alternative β-rich oligomeric form (*11−13*). The α-rich form can give rise to long straight amyloid fibrils, and the mechanism of formation of long straight fibrils has been studied extensively (*12−15*). The β-rich form gives rise to worm-like fibrils (*16, 17*), but relatively little is known about the mechanism of formation of worm-like fibrils. It is important to understand how the prion protein misfolds to adopt the alternative β-rich conformation (*11*) and how such misfolding leads to the formation of ordered amyloidogenic aggregates.

In vitro aggregation of the prion protein has been studied extensively using the recombinant prion protein expressed in bacteria. The recombinant protein has a disulfide bond between C179 and C214 as in mammalian protein, but glycosylation at N181 and N193 and the GPI anchor at the C-terminus are absent. The recombinant mouse prion protein serves as an excellent model for studying the mechanism underlying the conversion of PrP^C to PrP^{Sc} because it has been shown that in the presence of specific lipids and RNA, it can be converted to the infectious prion isoform (*18*). The prion protein has an unstructured N-terminal domain (residues 23−120) and a folded C-terminal domain (residues 121−231) (Figure 1), but in most studies so far, a truncated form of the prion protein (either residues 90−231 or residues 120−231) has been used because residues 23−90 have been shown not to be essential for prion transmission (*2, 19*). Nevertheless, the N-terminal region may still be important both in prion pathogenesis and in defining the prion strains.

A lack of PrP^c function, due to conversion of PrP^c to PrP^{Sc}, appears not to be responsible for prion-related disorders (*20, 21*). The deposition of PrP^{Sc} in the brain does not show a strict correlation with any prion disease phenotype, which suggests that PrP^{Sc} itself may not be toxic (*22−25*). In the case of other amyloidogenic diseases, oligomeric intermediates, formed initially during the conversion of the monomeric state into amyloid fibrils, seem to be the toxic species (*26−29*). It is possible that prion-mediated toxicity and infectivity are also caused by an intermediate oligomeric state formed during the conversion of PrP^c to PrP^{Sc}. It therefore becomes imperative to characterize the intermediate

*To whom correspondence should be addressed. Telephone: 91-80-23666150. Fax: 91-80-23636462. E-mail: jayant@ncbs.res.in.

FIGURE 1: Structure of the folded C-terminal domain (residues 121−231) of mouse prion protein. The N-terminal segment (residues 23−120) is presumably unstructured (*2*). The locations of residues M129, F175, and D178 that were mutated to V, W, and N, respectively, are shown. The structure was drawn from Protein Data Bank entry 1AG2 using PyMOL (http://www.pymol.org) (*51*).

prefibrillar aggregates and their role in the amyloidogenic aggregation of the prion protein, which might represent the conversion of PrP^c to PrP^{Sc}.

In the aggregation reactions of many proteins, prefibrillar aggregates seem to accumulate at the expense of monomers, before the formation of mature amyloid fibrils commences (*30, 31*). The exact role of these prefibrillar aggregates in the overall pathway of amyloid fibril formation is, however, not clear. The transient nature and the limited stability of these prefibrillar aggregates make it difficult to be capture and study them.

The aggregation reaction of the mouse prion protein has been shown to involve prefibrillar oligomers (*13*). An important goal of studies of the aggregation of the prion protein is to establish the role of these prefibrillar oligomers in the overall mechanism of fibril formation, as well as to explore structural heterogeneity therein. A previous study (*16*) of the formation of worm-like fibrils by the full-length mouse prion protein, at pH 2 in the presence of 150 mM NaCl, has shown that the α-rich monomer of the protein exists in a slow equilibrium with a β-rich oligomer. The relative amounts of β-rich oligomer and monomer could be varied either by varying the total protein concentration at a fixed NaCl concentration (*16*) or by varying the NaCl concentration at a fixed total protein concentration (*17*). In both cases, the observed rate constant of fibril formation was found to be linearly dependent on the concentration of β-rich oligomer, but the rate constants and their dependencies were different. This result suggested that the structural composition of the β-rich oligomer changes with salt concentration and/or that the β-rich oligomer comprises at least two subpopulations of molecules (*17*).

In this study, we show that the β-rich oligomer does indeed comprise two subpopulations of oligomers that differ in their secondary structures. The fractional amounts of the larger oligomer (oligomer L) and the smaller oligomer (oligomer S) can be tuned by changing the concentration of NaCl in the aggregation buffer as well as by introducing single-point mutations into the protein. The mutant proteins used in this study are M129V, F175W, and D178N, in which the mutations are present in the folded C-terminal domain (Figure 1). The apparent rate constant of worm-like amyloid fibril formation increases with an increase in the concentration of oligomer L but remains unaffected by a change in the concentration of oligomer S. It therefore appears that oligomer L is on the direct pathway of worm-like amyloid fibril formation by the mouse prion protein. On the other

hand, oligomer S appears to be an off-pathway oligomer that is formed in competition with oligomer L and that cannot directly transform into fibrils.

EXPERIMENTAL PROCEDURES

Protein Expression and Purification. The expression and purification of wild-type (wt) moPrP[1] have been described previously (*16*). Three mutant variants of moPrP, M129V, F175W, and D178N, were generated by site-directed mutagenesis and purified in a similar manner. The purity of each protein was confirmed by sodium dodecyl sulfate−polyacrylamide gel electrophoresis and electrospray ionization mass spectrometry. The purified proteins were stored in 10 mM sodium acetate buffer (pH 4), at −80 °C, as described previously (*16*).

Buffers, Solutions, and Experimental Conditions. All reagents used for the experiments were of the highest purity grade available from Sigma. The protein in 10 mM sodium acetate buffer (pH 4) was diluted 2-fold with 2× aggregation buffer, so that the protein was finally in 50 mM glycine buffer containing the desired concentration of NaCl at pH 2. The final protein concentration used for most of the experiments was 25 μM, except for the FTIR studies, and other studies as mentioned specifically.

Aggregation Studies. The aggregation process was monitored by measurement of ThT fluorescence. For all the measurements, the protein was first incubated for 1 h in aggregation buffer at 25 °C. After incubation for 1 h, the protein was transferred into a tube in the heating block, preset at either 50 ± 0.5 or 60 ± 0.5 °C. The same heating block was used for all the experiments to reduce variability. The temperature jump of the protein solution was complete within 4 min of incubation in the heating block. At different time points of aggregation, aliquots of the protein sample were withdrawn for analysis by the measurement of ThT fluorescence.

Thioflavin T Fluorescence Assay. For the assay, final concentrations of 2 μM protein and 20 μM ThT were used. A calculated amount of protein was withdrawn from the sample and added to the ThT-containing assay solution [50 mM Tris (pH 8)]. ThT fluorescence was measured using a Fluoromax-3 spectrofluorimeter (Jobin Yvon). The following experimental settings were used: excitation wavelength, 440 nm; emission wavelength, 482 nm; excitation bandwidth, 1 nm; and emission bandwidth, 10 nm. Measurements were taken within 30 s of the addition of the protein to the assay solution.

Size Exclusion Chromatography. The hydrodynamic properties of moPrP were studied by gel filtration on a Waters Protein Pak 300-SW column using an Akta (GE) chromatography system. The fractionation range of the 15.1 mL column was 10−300 kDa, and the void volume was determined to be 6.2 mL. Each protein sample was equilibrated in 50 mM glycine buffer (pH 2) containing the desired amount of NaCl for 1 h prior to the acquisition of the chromatogram. Before injection of 50 μL of the protein solution, the column was equilibrated with 4 column volumes of the same buffer. In the case of the native protein, the column was equilibrated with 100 mM sodium acetate buffer (pH 4). A flow rate of 0.72 mL/min was used.

Circular Dichroism Spectroscopy. A Jasco J-720 spectropolarimeter was used for the far-UV CD measurements. A cuvette with a path length of 2 mm was used. For the acquisition of

---

[1]Abbreviations: moPrP, mouse prion protein; ThT, thioflavin T; CD, circular dichroism; FTIR, Fourier transform infrared; AFM, atomic force microscopy.

spectra, the β-rich oligomers were separated using size exclusion chromatography into oligomer L (which elutes in the void volume) and oligomer S (which just enters into the column). These separated oligomers were concentrated to ~5 μM using a 10 kDa Centricon (Millipore Corp.). Spectra were recorded in the wavelength range of 200−250 nm. The following instrument settings were used: step resolution, 1 nm; scan speed, 100 nm/min; and bandwidth, 1 nm. Each spectrum was averaged for more than 30 scans.

Fourier Transform Infrared Spectroscopy. FTIR measurements were taken using a Thermo Nicholet-6700 FTIR spectrometer (Thermo Scientific) equipped with a liquid nitrogen-cooled MCT detector. Buffers (see above) created in H_2O were used. The spectrometer was purged with ultrapure nitrogen gas. Oligomers were formed with 25 μM protein (pH 2) in the presence of 150 mM NaCl. The solutions were concentrated ~10-fold using Centricons (Millipore Corp.) with a 10 kDa cutoff. The concentrated samples were applied to a diamond crystal, and spectra were recorded in the attenuated total reflectance (ATR) mode at a resolution of 4 cm^{-1}. Before the acquisition of sample data, the buffer spectrum was recorded under identical conditions and was used as the blank; 256 scans were averaged.

Atomic Force Microscopy. For the AFM studies of worm-like fibrils, 25 μM protein in 50 mM glycine buffer (pH 2) containing 150 mM NaCl was heated to 60 °C. At the appropriate time of aggregation, an aliquot was withdrawn and diluted to 0.5 μM in the same buffer. For AFM studies of the β-rich oligomer, 25 μM protein was incubated for 1 h in 50 mM glycine buffer (pH 2) containing 150 mM NaCl, after which an aliquot was withdrawn and diluted to 0.1 μM. The diluted sample was applied to a freshly cleaved mica sheet and incubated for 1 min. The mica surface was then rinsed three times with filtered water at pH 2 and dried under vacuum for 45 min before it was scanned. The AFM images were obtained using a PicoPlus AFM instrument (Molecular Imaging Inc.) operating in the noncontact mode, as described previously (*16*).

RESULTS

Characterization of Oligomer L and Oligomer S Formed by Wild-Type moPrP. In a previous study (*16*), gel filtration chromatography had shown that moPrP oligomerizes into a β-rich oligomer with a reduction in pH in the presence of 150 mM NaCl. At this NaCl concentration and at a final protein concentration of 25 μM, ~97% of the protein was found to have formed the β-rich oligomer. On the gel filtration column, which has a fractionation range of 10−300 kDa, some of the β-rich oligomer was seen to elute out in the void volume, while the remaining oligomer elutes out at a volume corresponding to a protein of molecular mass in the range of 200−300 kDa (Figure 2a). From the elution profile, it therefore appears that the β-rich oligomer comprises an oligomer L that elutes out in the void volume and an oligomer S that elutes out at a larger volume. In earlier studies (*16, 17*), the roles of the oligomer L and oligomer S components of the heterogeneous β-rich oligomer, in fibril formation, had not been delineated.

For 25 μM protein in 150 mM NaCl, deconvolution of the areas under the monomer, oligomer S, and oligomer L peaks in the size exclusion chromatogram (Figure 2a) indicated that monomer, oligomer S, and oligomer L constitute 6, 59, and 35%, respectively, of the total protein. Oligomer L and oligomer S were separated by size exclusion chromatography conducted in
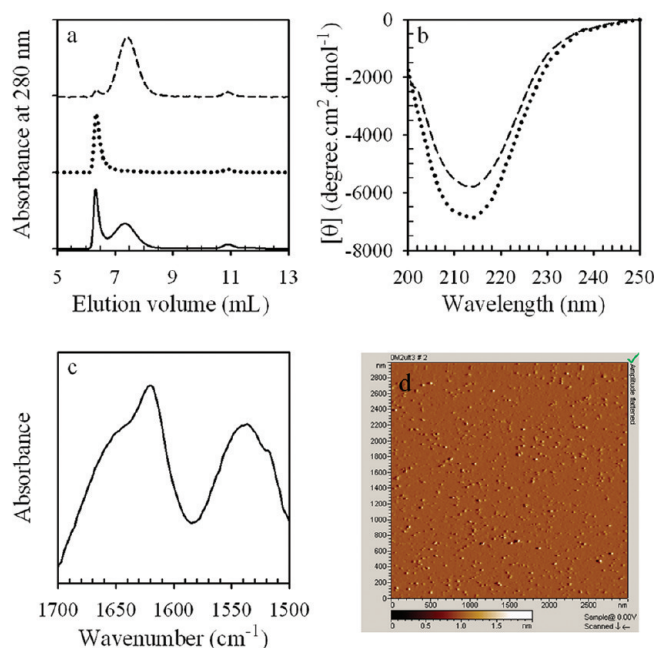

FIGURE 2: Characterization of the small (oligomer S) and large (oligomer L) components of the β-rich oligomer formed by wt moPrP at pH 2. (a) Size exclusion chromatograms in 50 mM glycine buffer containing 150 mM NaCl (pH 2) of total β-rich oligomer (—), of purified oligomer L (···), and purified oligomer S (---). (b) Far-UV CD spectra of oligomer L (···) and oligomer S (---). (c) FTIR spectrum of total β-rich oligomer (containing ~40% oligomer L and ~60% oligomer S). (d) AFM image (amplitude mode) of total β-rich oligomer (containing ~40% oligomer L and ~60% oligomer S).

the presence of 150 mM NaCl and were characterized structurally using circular dichroism (CD) and Fourier transform infrared (FTIR) spectroscopy. To prepare pure oligomer L, only the protein that eluted out in the first half of the oligomer L elution peak was collected. To prepare pure oligomer S, only the protein that eluted out in the second half of the oligomer S elution peak was collected. Figure 2a shows the elution profile of separated oligomer L as well as of oligomer S. Each oligomer preparation is seen to have <15% contamination of the other oligomer. Upon prolonged incubation of purified oligomer L or oligomer S in the presence of 150 mM NaCl, it was found that re-equilibration between the oligomers and monomer was slow, and that <25% of each oligomer had transformed into the other even after incubation for 7 h. Re-equilibration in 150 mM NaCl was especially very slow starting from the separated oligomer S. For 5 and 25 μM oligomer S, the relative amounts of oligomer S, oligomer L, and monomer were found to be ~92, 4, and 4%, respectively, and did not change from 1 to 24 h. Re-equilibration in 150 mM NaCl was comparatively faster starting from oligomer L. For 5 μM purified oligomer L, a slow disaggregation leading to the formation of oligomer S was observed, and the relative amount of oligomer S increased to 10% after incubation for 7 h. Interestingly, the amount of monomer remained constant (~3%) during this incubation (data not shown).

Spectroscopic characterization of oligomer L and oligomer S was conducted within 30 min of separation. The far-UV CD spectra of oligomers L and S exhibit minima at ~214 nm, suggesting that both are β-rich (Figure 2b). The mean residue ellipticity of oligomer L is, however, higher than that of oligomer S. In a FTIR spectrum, a peak in the region of 1613−1643 cm^{-1} corresponds to β-sheet rich structures and a peak at ~1650 cm^{-1} represents α-helix and/or random coil structures (*32−34*). The FTIR spectrum
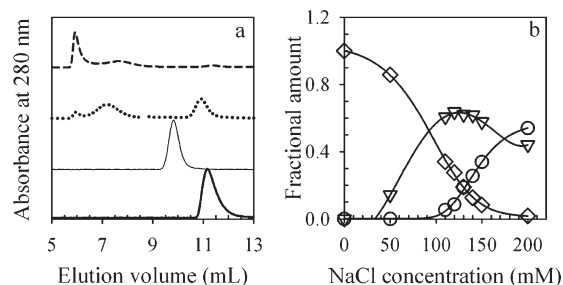
FIGURE 3: Salt-induced modulation of the relative amounts of oligomer L, oligomer S, and monomer. (a) Size exclusion chromatograms of native protein at pH 4 (thick solid line), protein in 50 mM glycine buffer (pH 2) (thin solid line), protein in 50 mM glycine buffer (pH 2) containing 120 mM NaCl (dotted line), and protein in 50 mM glycine buffer (pH 2) containing 200 mM NaCl (dashed line). In each case, the concentration of the protein was 25 μM. (b) Fractional amounts of oligomer L ($\bigcirc$), oligomer S ($\triangledown$), and monomer ($\Diamond$) at different NaCl concentrations at pH 2. The fractional amount of each form was calculated by integration of the area under the respective peak in the size exclusion chromatogram.

of total β-rich oligomer (containing oligomer L and oligomer S) (Figure 2c) has a peak at ~1620 cm^{-1} and a shoulder at ~1650 cm^{-1}. FTIR spectra of the individual oligomers could not be recorded because of the time necessary to concentrate the samples sufficiently for measuring the spectra, and because of the uncertainty about how such sample concentration would affect the rates of equilibration between the oligomers.

The AFM image of total β-rich oligomer (containing oligomer L and oligomer S) (Figure 2d) shows only spherical oligomers that are highly heterogeneous in their sizes, as expected from the size exclusion chromatograms (Figure 2a). No fibrillar structures are seen, indicating that both oligomer L and oligomer S are spherical and not fibrillar.

NaCl-Induced Oligomerization of the Mouse Prion Protein at Low pH. Figure 3a shows that at pH 2, and in the absence of any added salt, moPrP remains monomeric at a concentration of 25 μM. The size exclusion profiles of the protein at pH 2 and of the native protein at pH 4 indicate that the protein at pH 2 is monomeric but is less compact than the native protein at pH 4. An earlier study (*16*) had shown that the protein at pH 2 is α-rich but has lost some of the secondary structure present in the native protein. Upon addition of NaCl at pH 2 and 25 °C, the protein transforms into the β-rich oligomer ensemble, which has been shown to be stabilized differentially by different salts (*17*). Size exclusion chromatography of 25 μM protein in the presence of NaCl shows that the relative amounts of monomer, oligomer L, and oligomer S are different at different NaCl concentrations (Figure 3a). In 120 mM NaCl, ~9% of the protein elutes as oligomer L, 64% as oligomer S, and the remaining ~27% as monomer. In 200 mM NaCl, oligomer L, oligomer S, and monomer constitute ~54, ~44, and <2% of the total protein, respectively. At either salt concentration, the final distribution of monomer, oligomer S, and oligomer L is reached within 1 h of addition of salt, and the distribution does not change over the next 4 h.

In Figure 3b, the fractional populations of oligomer L, oligomer S, and monomer are plotted versus NaCl concentration. The fractional amounts of the three forms were calculated using the areas under the respective peaks in the size exclusion chromatography elution profiles. The amount of monomer decreases, and the amount of oligomer L as well as oligomer S increases, in a sigmoidal manner with an increasing concentration of NaCl.

The association reaction leading to the formation of oligomer S occurs at a lower salt concentration than that leading to the formation of oligomer L. Hence, only monomer and oligomer S are seen in 50 mM NaCl.

Effect of Salt on the Kinetics of Formation of Fibrils from the β-Rich Oligomer. The oligomers formed either in the presence or in the absence of NaCl transform into worm-like fibrils. The transformation is very slow at 25 °C but becomes faster at higher temperatures (*16*). Figure 4a shows the thioflavin T (ThT) fluorescence-monitored kinetics of the formation of worm-like amyloid fibrils from β-rich oligomers at NaCl concentrations of 110, 140, and 200 mM. At each salt concentration, no lag phase is apparent and the kinetics appear to be monophasic. The observed rate is seen to increase with an increase in NaCl concentration.

In panels b and c of Figure 4, the apparent rate constant of worm-like fibril formation is plotted versus the fractional amounts of oligomer L and oligomer S. The fractional amounts of oligomer L and oligomer S were varied by varying the NaCl concentration. The apparent rate constant increases linearly with an increase in the fractional amount of oligomer L present prior to the start of fibril formation (Figure 4b). The amount of oligomer S does not change appreciably in the range of NaCl concentration that leads to an ~10-fold increase in the rate constant (Figure 4c).

The Relative Amounts of Oligomer S and Oligomer L Formed by Different Mutant Forms of moPrP Are Different. The human PrP gene exists in two major allelic forms that encode either methionine or valine at residue position 129 (*35*). The mutant variant D178N with M at residue position 129 is linked to fatal familial insomnia (*35*). These different variants of the prion protein are linked to different disease susceptibilities, incubation periods, and phenotypes (*35*). The effects of these mutations on the formation of long straight fibrils have been studied in detail (*36, 37*), but their effects on the formation of worm-like fibrils have not been studied.

Oligomerization of the wt protein and three mutant forms of moPrP, namely, M129V, F175W, and D178N, were studied using gel filtration chromatography (Figure 5). Each of the three mutant variants forms β-rich oligomer at pH 2 in the presence of 150 mM NaCl at 25 μM protein (Figure 5a). Interestingly, the total amount of β-rich oligomer varies across the mutant proteins. In Figure 5b−e, the dependencies on protein concentration of the fractional amounts of monomer, oligomer S, and oligomer L as determined from the areas under the elution profiles from size exclusion chromatography are shown for the wt protein, M129V, F175W, and D178N.

As seen for the wt protein (*16*), the oligomerization leading to β-rich oligomer formation by M129V saturates at a protein concentration of 25 μM (Figure 5b,c) but saturates at higher protein concentrations in the case of the F175W and D178N mutants (Figure 5d,e). The relative amounts of oligomer L and oligomer S for M129V and F175W at saturating protein concentrations are similar to that seen for the wt protein (data not shown). Interestingly, in the case of D178N, the β-rich oligomer comprises mostly oligomer S, and oligomer L is formed to a very small extent even at very high protein concentrations where the extent of oligomerization has saturated (Figure 5e).

Kinetics of Worm-like Fibril Formation by Different Mutant Variants of moPrP. Figure 6a shows the ThT fluorescence-monitored kinetics of the formation of worm-like amyloid fibrils from β-rich oligomers of wt protein, as well as of M129V, F175W, and D178N, at 150 mM NaCl and 25 μM protein.
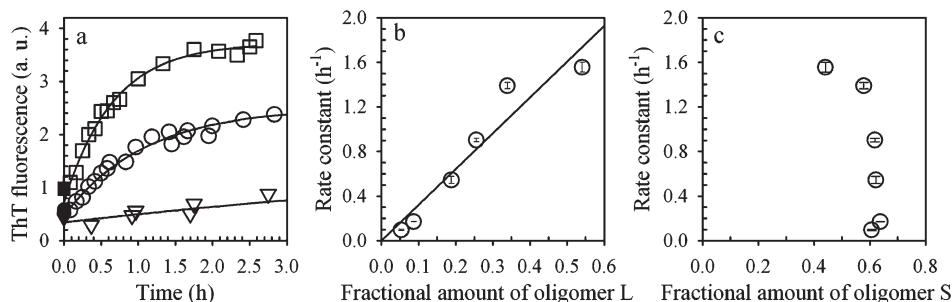
FIGURE 4: Effect of NaCl on the kinetics of amyloid fibril formation by 25 μM moPrP at pH 2 and 50 °C. NaCl concentrations of 110, 120, 130, 140, 150, and 200 mM were used. (a) ThT fluorescence-monitored kinetic traces of amyloid fibril formation by 25 μM protein in the presence of 110 ($\triangledown$), 140 ($\bigcirc$), and 200 mM NaCl ($\square$) at pH 2 and 50 °C. (b and c) Dependencies of the apparent rate constant of worm-like amyloid fibril formation on the fractional amounts of oligomer L and oligomer S, respectively. The apparent rate constants were determined from single-exponential fits of the kinetic traces. The error bars represent the spreads in the values obtained from two independent experiments.
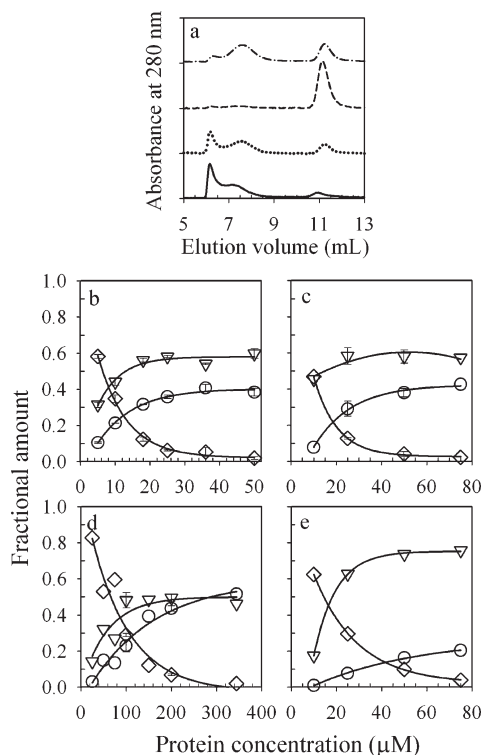

FIGURE 5: Mutational modulation of oligomer S and oligomer L formation. (a) Size exclusion chromatograms in 50 mM glycine buffer containing 150 mM NaCl (pH 2) for the wt protein (—), M129V (···), F175W (---), and D178N (−·−). The protein concentration was 25 μM in each case. (b–e) Fractional amounts of monomer ($\diamond$), oligomer S ($\triangledown$), and oligomer L ($\bigcirc$) formed at different protein concentrations for the wt protein (b), M129V (c), F175W (d), and D178N (e). In each case, the amounts of monomer and oligomers were calculated by integrating the areas under the elution peaks. The error bars represent the spreads in the values obtained from two independent experiments.

As seen previously for the wt protein (*16, 17*), no lag phase is apparent, and the kinetics appear to be monophasic for each of the mutant variants. The apparent rate constant for each variant is seen to be different. At 25 μM protein, the apparent rates of formation of worm-like fibrils by the mutant proteins are slower than that by the wt protein (Figure 6b). It is important to note that the fractional amount of oligomer L is different for the different proteins at this protein concentration (Figure 5a). Interestingly, the apparent rate constant of worm-like fibril formation by the wt protein and the different mutant variants is dependent linearly on the fractional amount of oligomer L present prior to the start of worm-like

amyloid fibril formation (Figure 6c). This result is in accordance with the result for the wt protein when the fractional amount of oligomer L was varied by varying the NaCl concentration (Figure 4b) and confirms that oligomer L acts as the direct precursor for the formation of worm-like fibrils by moPrP at low pH.

AFM Studies of the Worm-like Amyloid Fibrils Formed by the wt Protein and Its Mutant Variants. Figure 7 shows atomic force microscopy (AFM) images of the worm-like amyloid fibrils formed by the wt protein and its different mutant forms, at a time corresponding to three time constants of the ThT fluorescence-monitored kinetics. In the case of D178N, the kinetics of aggregation were very slow; hence, AFM images were acquired after samples had been heated for 15 h at 60 °C before the completion of the reaction. In the case of the wt protein as well as for each of the mutant forms, elongated, curly worm-like nanostructures are seen to form. Their mean diameters, as determined from the *Z* heights on AFM mica, are similar (~2 nm). The lengths of the worm-like amyloid fibrils are, however, seen to vary. The worm-like fibrils formed by the wt protein and M129V are similar in length, while the fibrils formed by F175W are very heterogeneous in their lengths, with some fibrils being significantly longer that those formed by the wt protein or by M129V. In the case of D178N, as expected from a low ThT fluorescence signal at 15 h, very few fibrils are seen to form, and spherical oligomers appear to represent the predominant form present (Figure 7d, inset).

DISCUSSION

Soluble small oligomers have been observed during the course of the formation of amyloid fibrils by many proteins, including moPrP (*17*). The exact role of oligomers in the aggregation process of the prion protein, as well as for many other proteins, is, however, still unclear. For many proteins, the observation that internal order increases from the oligomers to fibrils suggests that the oligomers are on the pathway of fibril formation (*38−40*). On the other hand, there is evidence suggesting that the oligomers are off-pathway structures in the aggregation reactions leading to fibril formation (*13, 41−43*). There is little direct kinetic evidence defining the roles of such oligomers on the pathway of fibril formation of the prion protein (*16, 17*). In this study, the mouse prion protein has been shown to form multiple oligomeric forms at pH 2. Defining the roles of these oligomers on the pathway of prion protein aggregation is important not only for understanding the mechanism of prion protein aggregation but also for gaining insight into prion strain diversity (*5, 6, 44*).
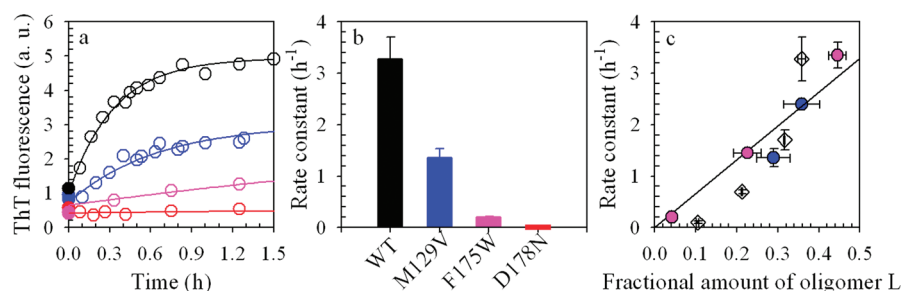
FIGURE 6: Effect of mutation on the apparent rate constant of worm-like amyloid fibril formation. The apparent rate constants were measured in 50 mM glycine buffer containing 150 mM NaCl at pH 2 and 60 °C. (a) Kinetics of worm-like amyloid fibril formation monitored by ThT fluorescence for wt protein (black circles), M129V (blue circles), F175W (pink circles), and D178N (red circles) at 25 μM. (b) Apparent rate constants of worm-like amyloid fibril formation by wt protein (black bar), M129V (blue bar), and F175W (pink bar) at 25 μM. In the case of D178N, it was not possible to measure the rate at 25 μM concentration because of very slow aggregation kinetics; hence, a red bar has been put at ~0 to show that kinetics were very slow for this variant. (c) Dependence of the apparent rate constant on the fractional amount of oligomer L for wt protein (black diamonds), M129V (blue circles), and F175W (pink circles). The apparent rate constants were determined from single-exponential fits of the kinetic traces. The error bars represent the spreads in the values obtained from two independent experiments.
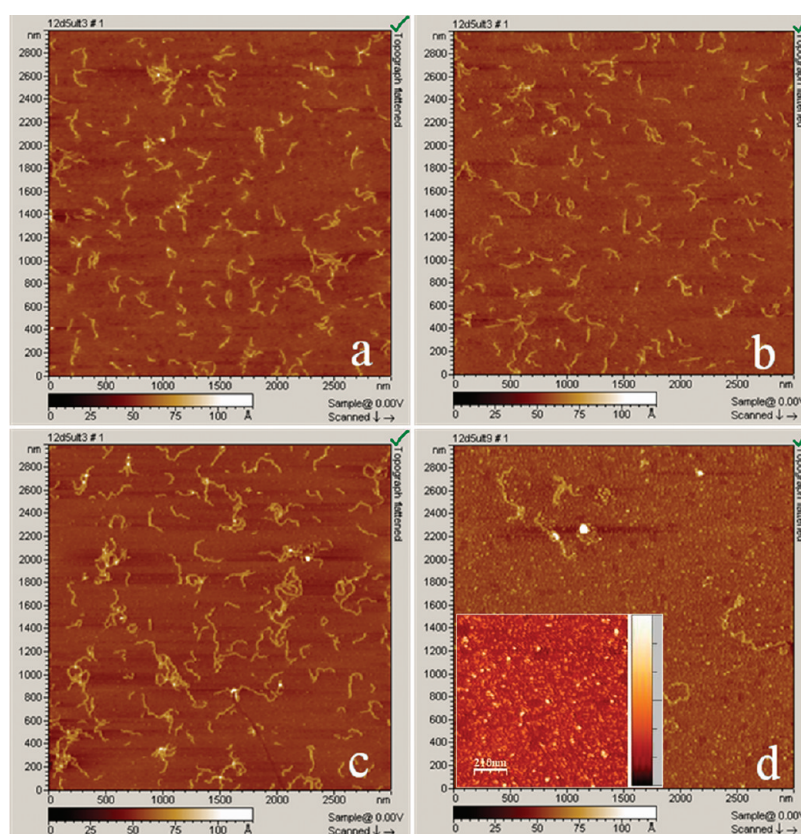

FIGURE 7: AFM images of worm-like amyloid fibrils formed by wt moPrP and its mutant variants. In each case, 25 μM protein was heated to 60 °C in 50 mM glycine buffer containing 150 mM NaCl (pH 2). Panels a-d represent AFM images (topography mode) of worm-like amyloid fibrils formed by wt protein, M129V, F175W, and D178N, respectively. AFM images were acquired at a time corresponding to three time constants of the ThT fluorescence-monitored kinetics, except for D178N. For this protein, the AFM image was acquired after the sample had been heating for 15 h at 60 °C, to avoid fragmentation of the protein chain. The inset shows a zoomed AFM image of D178N oligomers. The $X-Y$ scale bar shown in the inset is 210 nm, and the Z scale is from 0 to 3 nm.

The β-Rich Oligomer of moPrP Consists of Two Distinct Subpopulations. moPrP forms a β-rich oligomer, which exists in equilibrium with the α-rich monomer in a concentration-dependent manner, at low pH in the presence of salt (Figure 5). An earlier study (*16*) had shown that the β-rich oligomer is the direct precursor for worm-like fibril formation. In this study, the β-rich oligomer formed at pH 2 has been shown to consist of two distinct oligomeric subpopulations, oligomer L and oligomer S. Oligomers L and S differ in their sizes as well as in their β-sheet contents (see above); oligomer L is larger and has a higher β-sheet content than oligomer S. A non-zero ThT fluorescence signal of the β-rich

oligomer suggests that a few ThT binding sites are present in these oligomers (Figures 4a and 6a).

Previous studies (*45−47*) had indicated that discrete soluble oligomeric species are generated upon thermal unfolding of the prion proteins, at low pH (~3.5) in the presence of salt. The role of these structurally distinct oligomers in the kinetics of fibril formation has, however, remained elusive. Although their far-UV CD spectra are similar, the oligomers seen in the previous studies differ in their FTIR spectra from the oligomers observed in this study. The aggregation conditions used in this study (pH 2, 150 mM NaCl, 25 °C) are different from those used in the
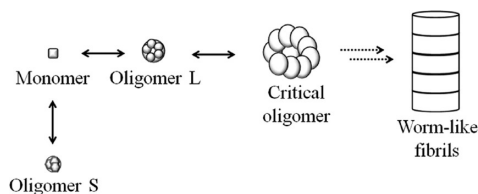
FIGURE 8: Pathway of formation of worm-like fibrils by the mouse prion protein. On- and off-pathway oligomers are populated during the formation of worm-like amyloid fibrils by moPrP. Oligomer S is smaller and off-pathway and has an internal structure that is different from that of the larger, on-pathway oligomer L. The worm-like fibrils form from oligomer L via a critical oligomer identified in an earlier study (*16*). The pathway of formation of long straight fibrils via an alternative pathway under different aggregation conditions is not shown.

previous studies (pH ~3.5, different ionic strength, 37−45 °C). It therefore appears that high structural heterogeneity exists at the oligomeric stage during the aggregation of prion proteins. It remains to be seen whether the oligomers formed at pH ~3.5 form sequentially from monomer (*45*) or whether they form on parallel pathways (*46, 47*). Furthermore, it is crucial to establish the role of these oligomeric subpopulations in the overall process of fibril formation by the prion proteins.

Oligomer L and Oligomer S Are Formed on Parallel Pathways. There are two possible ways by which oligomer L and oligomer S could form from the monomer. According to pathway I (S ↔ M ↔ L), oligomer S forms in an off-pathway manner with respect to the pathway of formation of oligomer L. According to pathway II (M ↔ S ↔ L), oligomer S is a productive intermediate on the pathway of formation of oligomer L. A key observation that makes it possible to rule out pathway II is that the final distribution of monomer, oligomer S, and oligomer L, at any NaCl concentration between 110 and 200 mM (Figure 3b), is reached within 1 h of the addition of NaCl and does not change upon further incubation for up to 4 h. Hence, both oligomers are fully formed from monomer within 1 h. Thus, if oligomer S were a productive intermediate (pathway II), then isolated oligomer S should re-equilibrate to form oligomer L within 1 h of incubation. Instead, it is seen that isolated oligomer S has neither transformed into oligomer L nor dissociated into monomer at 5 or 25 μM protein, even after incubation for 20 h. Oligomer S cannot, therefore, be a productive intermediate on the pathway from monomer to oligomer L. The conclusion is supported by the observation that in 50 mM NaCl, only monomer and oligomer S are present (see Results). If oligomer S were a productive intermediate, then oligomer L would also be expected to be present.

It therefore appears that pathway I is appropriate for describing the oligomerization of moPrP at pH 2 (Figure 8). The observation that when oligomer L is isolated at a concentration of 5 μM it is slowly transformed into oligomer S without any transient accumulation of monomer (see Results), suggests that the dissociation of oligomer L into monomer is rate-limiting in the transformation.

The Relative Stabilities of Oligomers S and L Can Be Modulated by Salt Concentration and Mutation. The data in Figures 3 and 5 suggest that the equilibria for the formation of oligomer S and oligomer L from monomer are affected strongly not only by a change in salt concentration but also by mutation. A previous study (*17*) had shown that anions bind to the prion protein and thereby modulate the structure of the β-rich oligomers. This study suggests that anion binding affects the relative

stabilities of oligomer S and oligomer L. The apparent binding constants for the association of monomer to form oligomer S and oligomer L appear to be affected very significantly by single-amino acid residue changes in sequence. Unfortunately, in the absence of any structural data for oligomers S and L, it is difficult to understand the effects of the mutations and of salt concentration on the conformational equilibria.

Oligomer L, and Not Oligomer S, Acts as the Direct Precursor for Worm-like Fibril Formation. Either oligomer could conceivably serve as the starting point for worm-like amyloid fibril formation. The observation that the apparent rate constant of worm-like amyloid fibril formation increases linearly with the fractional amount of oligomer L and the observation that the fractional amount of oligomer S does not change (Figure 4b,c) over the range of salt concentration over which the observed rate constant changes indicate that the formation of worm-like amyloid fibrils proceeds directly from oligomer L, not from oligomer S. The linear dependence of the apparent rate constant on the oligomer L concentration makes it very unlikely that dissociation of oligomer L to smaller oligomers leads to a form competent to form worm-like amyloid fibrils. If a dissociated product of oligomer L were the precursor of worm-like fibril formation, then the dependence of the apparent rate on oligomer L concentration would not be expected to be linear, because the degree of dissociation into the smaller oligomer would not have a linear dependence on oligomer L concentration.

The on-pathway role of oligomer L is evident also from the mutational studies. Each mutant variant forms oligomer S and oligomer L at low pH (Figure 5). The apparent rate of formation of worm-like fibrils from the β-rich oligomer of each of the mutant proteins is, however, slower than that from the wt protein (Figure 6b). Interestingly, the amounts of the two β-rich oligomers are differentially dependent on the protein concentration for the different mutant proteins, and the apparent rate constant of worm-like fibril formation is proportional to the fractional amount of oligomer L (Figure 6c), as seen for the wt protein at different NaCl concentrations. It has been shown for the mouse prion protein in this study, as shown earlier for the SH3 domain of PI3 kinase (*48*), that amyloid fibril formation is accelerated by the formation of critical oligomers.

In the case of D178N, the β-rich oligomer consists largely of oligomer S with a small amount of oligomer L (Figure 5a); consequently, this mutant variant forms very few fibrils (Figure 7d). The predominant protein aggregates appear to be spherical oligomers, as seen in the AFM image (Figure 7d). This observation suggests that this particular mutation leads to destabilization of oligomer L, and hence, fibrillation is very slow. The observation that much more oligomer S than oligomer L is formed in the case of D178N is in accordance with the placement of oligomer S off the pathway of formation of oligomer L from monomer (see above). If oligomer S were a productive oligomer intermediate leading directly to the formation of oligomer L, an increase in the amount of oligomer S would have led to an increase in the amount of oligomer L, but this observation by itself would not have been able to rule out the possibility that both oligomers are formed sequentially via pathway II, because it would have been possible to argue that this mutation might not affect the equilibrium between M and S but instead might affect the equilibrium between S and L on pathway II (see above).

Mutations Affect the Length of the Worm-like Amyloid Fibril. Different variants of the prion protein are linked to different disease susceptibilities, incubation periods, and phenotypes (*35*).

Hence, it was important to see whether the worm-like amyloid fibrils formed from the mutant variants, M129V, F175W, and D178N, are similar or different in structure. The AFM images show that the worm-like amyloid fibrils formed by the wt protein and M129V are similar in length (Figure 7a,b) and are shorter than those formed by F175W and D178N (Figure 7c,d).

The lengths of worm-like fibrils formed by different variants of moPrP are seen to correlate with the binding constants for oligomer L formation. The binding constants appear to be similar in the case of wt and M129V (Figure 5), and the fibrils formed by them are similar in length (Figure 7). Similarly, the binding constants for oligomer L formation appear to be similar for F175W and D178N, and they form fibrils of similar lengths. Interestingly, the binding constants for the formation of oligomer L by F175W and D178N appear to be lower than those for formation of oligomer L by the wt protein and M129V (Figure 5), and the fibrils formed by F175W and D178N are longer than those formed by wt and M129V. An earlier study (*16*) had suggested that the transformation of β-rich oligomer into worm-like fibrils involves a critical oligomer, and that the concentration of the critical oligomer determines the length of the fibrils formed. The correlation between the binding constant for oligomer L formation and the length of fibrils formed suggests that oligomer L participates in the formation of the critical oligomer (suggested in ref *16*). It appears that a higher binding constant for oligomer L formation is correlated with a larger number of critical oligomers, and thus, less protein would be left for growth of the critical oligomer into fibrils. Consequently, shorter fibrils will form. Conversely, a lower binding constant for the formation of oligomer L would lead to longer fibrils. At present, little is known about the structures of these critical oligomers, which are seen during the aggregation of not only the prion protein but also other amyloidogenic proteins (*31, 49*). The critical oligomers are populated very transiently, and it will be important in future work to stabilize and characterize them in detail. The heights of the worm-like fibrils formed by each of the variants are similar. Higher-resolution studies are needed to understand the differences between the worm-like fibrils formed from these variants.

Lastly, it is remarkable that studies of formation of amyloid fibrils by the full-length prion protein need to utilize strongly destabilizing conditions. The formation of long straight fibrils at pH 7 can be studied only in buffers containing 1−2 M GdnHCl, or both 1 M GdnHCl and 3 M urea, with 150 mM NaCl (*12−14, 36*) and invariably requires agitation of the solutions. The formation of worm-like fibrils does not require agitation but occurs to an easily measurable extent only at low pH. It appears that the formation of worm-like fibrils at pH 2 occurs because the protonation of a critical residue leads to destabilization of the native structure and to stabilization of an amyloidogenic conformation. Such a protonated amyloidogenic conformation would, of course, also exist at pH 7, but at such a low concentration that formation of oligomer L and worm-like fibrils would occur too slowly at pH 7 to be discernible. However, given that prion diseases are late-onset diseases (*35*), it is not unlikely that the slowness of aggregation of such protonated amyloidogenic conformations may be physiologically relevant.

CONCLUSION

Prefibrillar aggregates (oligomers and protofibrils) are recognized as important players in amyloid-related pathogenesis, such as in prion diseases (*50*). Previous studies had shown the formation

of discrete soluble oligomeric forms at low pH ($\sim$3.5) upon unfolding (*45−47*), but it was not clear whether these oligomers were generated by sequential or parallel pathways and whether they were the direct precursors for the formation of fibrils.

This study, conducted at pH 2, shows that moPrP utilizes alternative pathways to form two structurally distinct oligomers and that only one of the oligomers is on the direct pathway of worm-like fibril formation while the other one is off-pathway (Figure 8). The oligomerization of the prion protein is accompanied by a structural rearrangement of the native α-helical conformation to a β-rich state. Either a small change in the concentration of salt present during aggregation or a single-residue change in the protein sequence can lead to differential stabilization of the two distinct oligomeric forms. It is possible that similar phenomena lead to differences in phenotype during prion disorders or during pathology evolution. In the future, it will be important to study whether these structurally different oligomers are involved in the pathological diversity of the prion proteins.

REFERENCES

1. Prusiner, S. B. (1982) Novel proteinaceous infectious particles cause scrapie. *Science 216*, 136–144.
2. Prusiner, S. B. (1998) Prions. *Proc. Natl. Acad. Sci. U.S.A. 95*, 13363–13383.
3. Chiesa, R., and Harris, D. A. (2009) Fishing for Prion Protein Function. *PLoS Biol. 7*, 439–443.
4. Bremer, J., Baumann, F., Tiberi, C., Wessig, C., Fischer, H., Schwarz, P., Steele, A. D., Toyka, K. V., Nave, K., Weis, J., and Aguzzi, A. (2010) Axonal prion protein is required for peripheral myelin maintenance. *Nat. Neurosci. 13*, 310–320.
5. Collinge, J. (2001) Prion diseases of humans and animals: Their causes and molecular basis. *Annu. Rev. Neurosci. 24*, 519–550.
6. Aguzzi, A., and Polymenidou, M. (2004) Mammalian prion biology: One century of evolving concepts. *Cell 116*, 313–327.
7. Caughey, B., Baron, G. S., Chesebro, B., and Jeffrey, M. (2009) Getting a grip on prions: Oligomers, amyloids, and pathological membrane interactions. *Annu. Rev. Biochem. 78*, 177–204.
8. Wille, H., Michelitsch, M. D., Guénebaut, V., Supattapone, S., Serban, A., Cohen, F. E., Agard, D. A., and Prusiner, S. B. (2002) Structural studies of the scrapie prion protein by electron crystallography. *Proc. Natl. Acad. Sci. U.S.A. 99*, 3563–3568.
9. Govaerts, C., Wille, H., Prusiner, S. B., and Cohen, F. E. (2004) Evidence for assembly of prions with left-handed β-helices into trimmers. *Proc. Natl. Acad. Sci. U.S.A. 101*, 8342–8347.
10. Legname, G., Baskakov, I. V., Nguyen, H. O., Riesner, D., Cohen, F. E., DeArmond, S. J., and Prusiner, S. B. (2004) Synthetic mammalian prions. *Science 305*, 673–676.
11. Hornemann, S., and Glockshuber, R. (1998) A scrapie like unfolding intermediate of the prion protein domain PrP(121−231) induced by acidic pH. *Proc. Natl. Acad. Sci. U.S.A. 95*, 6010–6014.
12. Baskakov, I. V., Legname, G., Baldwin, M. A., Prusiner, S. B., and Cohen, F. E. (2002) Pathway complexity of prion protein assembly into amyloid. *J. Biol. Chem. 277*, 21140–21148.
13. Bocharova, O. V., Breydo, L., Parfenov, A. S., Salnikov, V. V., and Baskakov, I. V. (2005) *In vitro* conversion of full-length mammalian prion protein produces amyloid form with physical properties of PrP^{Sc}. *J. Mol. Biol. 346*, 645–659.
14. Baskakov, I. V. (2004) Autocatalytic conversion of recombinant prion proteins displays a species barrier. *J. Biol. Chem. 279*, 7671–7677.
15. Cobb, N. J., and Surewicz, W. K. (2009) Prion Diseases and Their Biochemical Mechanisms. *Biochemistry 48*, 2574–2585.
16. Jain, S., and Udgaonkar, J. B. (2008) Evidence for stepwise formation of amyloid fibrils by the mouse prion protein. *J. Mol. Biol. 382*, 1228–1241.

17. Jain, S., and Udgaonkar, J. B. (2010) Salt-induced modulation of the pathway of amyloid fibril formation by the mouse prion protein. *Biochemistry 49*, 7615–7624.

18. Wang, F., Wang, X., Yuan, C. G., and Ma, J. (2010) Generating a prion with bacterially expressed recombinant prion protein. *Science 327*, 1132–1135.

19. Parchi, P., Gambetti, P., Picardo, P., and Ghetti, B. (1998) Human prion diseases. In Progress in Pathology IV (Haddock, G. M., Ed.) pp 39−77, Churchill Livingstone, Edinburgh, U.K.

20. Bueler, H., Fischer, M., Lang, Y., Bluethmann, H., Lipp, H. P., DeArmond, S. J., Prusiner, S. B., Aguet, M., and Weissmann, C. (1992) Normal development and behaviour of mice lacking the neuronal cell-surface PrP protein. *Nature 356*, 577–582.

21. Bueler, H., Aguzzi, A., Sailer, A., Greiner, R. A., Autenried, P., Aguet, M., and Weissmann, C. (1993) Mice devoid of PrP are resistant to scrapie. *Cell 73*, 1339–1347.

22. Brandner, S., Isenmann, S., Raeber, A., Fischer, M., Sailer, A., Kobayashi, Y., Marino, S., Weissmann, C., and Aguzzi, A. (1996) Normal host prion protein necessary for scrapie-induced neurotoxicity. *Nature 379*, 339–343.

23. Lasmezas, C. I., Deslys, J. P., Robain, O., Jaegly, A., Beringue, V., and Peyrin, J. M.; et al. (1997) Transmission of the BSE agent to mice in the absence of detectable abnormal prion protein. *Science 275*, 402–405.

24. Mallucci, G., Dickinson, A., Linehan, J., Klohn, P. C., Brandner, S., and Collinge, J. (2003) Depleting neuronal PrP in prion infection prevents disease and reverses spongiosis. *Science 302*, 871–874.

25. Mallucci, G. R., White, M. D., Farmer, M., Dickinson, A., Khatun, H., Powell, A. D., Brandner, S., Jefferys, J. G., and Collinge, J. (2007) Targeting cellular prion protein reverses early cognitive deficits and neurophysiological dysfunction in prion-infected mice. *Neuron 53*, 325–335.

26. Caughey, B., and Lansbury, P. T. (2003) Protofibrils, pores, fibrils, and neurodegeneration: Separating the responsible protein aggregates from the innocent bystanders. *Annu. Rev. Neurosci. 26*, 267–298.

27. Kayed, R., Head, E., Thompson, J. L., McIntire, T. M., Milton, S. C., Cotman, C. W., and Glabe, C. G. (2003) Common structure of soluble amyloid oligomers implies common mechanism of pathogenesis. *Science 300*, 486–489.

28. Kayed, R., Sokolov, Y., Edmonds, B., McIntire, T. M., Milton, S. C., Hall, J. E., and Glabe, C. G. (2004) Permeabilization of lipid bilayers is a common conformation-dependent activity of soluble amyloid oligomers in protein misfolding diseases. *J. Biol. Chem. 279*, 46363–46366.

29. Chiti, F., and Dobson, C. M. (2006) Protein misfolding, functional amyloid, and human disease. *Annu. Rev. Biochem. 75*, 333–366.

30. Kodali, R., and Wetzel, R. (2007) Polymorphism in the intermediates and products of amyloid assembly. *Curr. Opin. Struct. Biol. 17*, 48–57.

31. Kumar, S., and Udgaonkar, J. B. (2010) Mechanisms of amyloid fibril formation by proteins. *Curr. Sci. 98*, 639–656.

32. Seshadri, S., Khurana, R., and Fink, A. L. (1999) Fourier transform infrared spectroscopy in analysis of protein deposits. *Methods Enzymol. 309*, 559–576.

33. Zandomeneghi, G., Krebs, M. R., McCammon, M. G., and Fandrich, M. (2004) FTIR reveals structural differences between native β-sheet proteins and amyloid fibrils. *Protein Sci. 13*, 3314–3321.

34. Susi, H. (1972) Infrared spectroscopy: Conformation. *Methods Enzymol. 26* (Part C), 455–472.

35. Prusiner, S. B. (2004) Prion biology and diseases, Cold Spring Harbor Monograph Series, Cold Spring Harbor Laboratory Press, Plainview, NY.

36. Apetri, A. C., Vanik, D. L., and Surewicz, W. K. (2005) Polymorphism at Residue 129 Modulates the Conformational Conversion of the D178N Variant of Human Prion Protein 90−231. *Biochemistry 44*, 15880–15888.

37. Jones, E. M., Surewicz, K., and Surewicz, W. K. (2006) Role of N-terminal Familial Mutations in Prion Protein Fibrillization and Prion Amyloid Propagation *in Vitro*. *J. Biol. Chem. 281*, 8190–8196.

38. Mukhopadhyay, S., Nayak, P. K., Udgaonkar, J. B., and Krishnamoorthy, G. (2006) Characterization of the formation of amyloid protofibrils from barstar by mapping residue-specific fluorescence dynamics. *J. Mol. Biol. 358*, 935–942.

39. Apetri, M. M., Maiti, N. C., Zagorski, M. G., Carey, P. R., and Anderson, V. E. (2006) Secondary structure of α-synuclein oligomers: Characterization by Raman and atomic force microscopy. *J. Mol. Biol. 355*, 63–71.

40. Kheterpal, I., Chen, M., Cook, K. D., and Wetzel, R. (2006) Structural differences in Aβ amyloid protofibrils and fibrils mapped by hydrogen exchange: Mass spectrometry with on-line proteolytic fragmentation. *J. Mol. Biol. 361*, 785–795.

41. Gosal, W. S., Morten, I. J., Hewitt, E. W., Smith, D. A., Thomson, N. H., and Radford, S. E. (2005) Competing pathways determine fibril morphology in the self-assembly of β2-microglobulin into amyloid. *J. Mol. Biol. 351*, 850–864.

42. Chen, Y. R., and Glabe, C. G. (2006) Distinct early folding and aggregation properties of Alzheimer amyloid-β peptides Aβ40 and Aβ42: Stable trimer or tetramer formation by Aβ42. *J. Biol. Chem. 281*, 24414–24422.

43. Hong, D. P., Ahmad, A., and Fink, A. L. (2006) Fibrillation of human insulin A and B chains. *Biochemistry 45*, 9342–9353.

44. Chien, P., Weissman, J. S., and DePace, A. H. (2004) Emerging principles of conformation-based prion inheritance. *Annu. Rev. Biochem. 73*, 617–656.

45. Rezaei, H., Eghiaian, F., Perez, J., Doublet, B., Choiset, Y., Haertle, T., and Grosclaude, J. (2005) Sequential generation of two structurally distinct ovine prion protein soluble oligomers displaying different biochemical reactivities. *J. Mol. Biol. 347*, 665–679.

46. Vendrely, C., Valadie, H., Bednarova, L., Cardin, L., Pasdeloup, M., Cappadoro, J., Bednar, J., Rinaudo, M., and Jamin, M. (2005) Assembly of the full-length recombinant mouse prion protein I. Formation of soluble oligomers. *Biochim. Biophys. Acta 1724*, 355–366.

47. Eghiaian, F., Daubenfeld, T., Quenet, Y., van Audenhaege, M., Bouin, A. P., van der Rest, G., Grosclaude, J., and Rezaei, H. (2007) Diversity in prion protein oligomerization pathways results from domain expansion as revealed by hydrogen/deuterium exchange and disulfide linkage. *Proc. Natl. Acad. Sci. U.S.A. 104*, 7414–7419.

48. Bader, R., Bamford, R., Zurdo, J., Luisi, B. F., and Dobson, C. M. (2006) Probing the mechanism of amyloidogenesis through a tandem repeat of the PI3-SH3 domain suggests a generic model for protein aggregation and fibril formation. *J. Mol. Biol. 356*, 189–208.

49. Modler, A. J., Gast, K., Lutsch, G., and Damaschun, G. (2003) Assembly of amyloid protofibrils via critical oligomers: A novel pathway of amyloid formation. *J. Mol. Biol. 325*, 135–148.

50. Silveira, J. R., Raymond, G. J., Hughson, A. G., Race, R. E., Sim, V. L., Hayes, S. F., and Caughey, B. (2005) The most infectious prion protein particles. *Nature 437*, 257–261.

51. DeLano, W. L. (2002) The PyMOL Molecular Graphics System, DeLano Scientific, San Carlos, CA.